PCCP

Accepted Manuscript

ROYAL SOCIETY OF CHEMISTRY

www.rsc.org/pccp

Adsorption of Choline Benzoate Ionic Liquid on Graphene, Silicene, Germanene and Boron-Nitride Nanosheets: A DFT perspective

Gregorio García,[a] Mert Atilhan,[b] and Santiago Aparicio*[a]

[a] Department of Chemistry, University of Burgos, 09001 Burgos, Spain

[b] Department of Chemical Engineering, Qatar University, P.O. Box 2713, Doha, Qatar

* Corresponding author: sapar@ubu.es (S. A.)

ABSTRACT: The adsorption of choline benzoate ([CH][BE]) ionic liquid (IL) on the surfaces of different hexagonal nanosheets has been studied by Density Functional Theory (DFT) methods. For this, the interaction mechanism, binding energies and electronic structure of [CH][BE] ionic liquid on four types of nanoshets, *i.e.,* graphene, silicene, germanene and boron-nitride, were estimated and compared. The adsorption of [CH][BE] ionic liquid on different nanosheets is mainly featured by van der Waals forces, leading to strong benzoate ion-surface π-stacking. Likewise, there is also an important charge transfer from the anion up to the sheet. The electronic structure analysis shows that Si and Ge based sheets bring the largest changes on HOMO and LUMO levels of choline benzonate. This paper provides new insights on the capability of DFT methods to shed useful information about adsorption of ionic liquids on nanosheets and how ionic liquid features could be tuned through the adsorption on suitable nanosheets.

Keywords: ionic liquids, nanostructures, graphene, silicene, germanene, boron nitride, DFT.

1. INTRODUCTION

Graphene could be defined as a single layer of carbon atoms with sp^2 hybridization arranged in a two dimensional (2D) honeycomb structure.[1, 2] Since its discovery in 2004,[3] a new area of research involving material science, physics, chemistry and biotechnology has emerged.[2, 4] Graphene is attractive because it shows many extraordinary characteristics, which are a direct consequence of its unique atomic structure, such as intrinsic zero-gap semiconductor character, high carrier mobility, high surface area, excellent thermal conductivity or biocompatibility.[2, 4, 5] Because of its remarkable properties, graphene-based applications have been reported in a wide range of areas, such as optoelectronic devices, energy generation, chemical sensors, or hybrid materials.[1, 2, 4] Likewise, the potential applications of graphene can be extended and task-specific tuned through the functionalization (or chemical absorption) of molecules and nanoparticles.[6] The mechanism of adsorption of relevant molecules, and also the changes in graphene properties upon molecular adsorption have been widely studied both using experimental and computational approaches.[6-8] Among the wide variety of molecules which could be absorbed on graphene surface, a very relevant field of study is the interaction of ionic liquids (ILs) with carbon nanostructures and their behavior with regard the carbon nanostructure, because of its importance both for basic science and for applied purposes.[8-12]

ILs are emerging as an attractive alternative to conventional organic solvents due to their especial chemical and physical properties: negligible vapor pressures, high thermal and chemical stability, non flammability or good solvent capacity for a wide range of organic, inorganic, polymeric and organometalic compounds, and the possibility of designing task-specific ILs through the suitable combination of cations and anions.[13] Therefore, ILs have been considered for applications in different technological fields such as lubrication, solvents extraction, catalytic processes or electrochemical applications.[14] In addition, the behavior of ILs with regard to graphene surfaces have also been studied, both using experimental and theoretical approaches, which have led to propose relevant applications in several technological fields, such as full cells, supercapacitors, solar cells or storage devices.[8, 10, 12, 15] As matter of fact, both theoretical and experimental studies have been conducted to elucidate the mechanism of interaction between ILs and graphene.[8, 10, 11, 15, 16, 17] Nevertheless, most available studies are limited to a reduced number of classic types of ILs, such as imidazol based ionic liquids.

Beyond the graphene sheets, other hexagonal 2D nanosheets such as silicene, germanene and boron-nitride analogues have also attracted increasing attention.[1, 18] Silicene

and germanene are the graphene counterparts based on silicon and germanium, which are both also elements of group IV. These materials also possess a honeycomb structure similar to graphene, and thus, they also show the most outstanding properties of graphene such as high carrier mobility, ferromagnetism or zero band gap.[1, 18] Alike, Si and Ge based nanosheets are expected to offer an alternative for the enhancement of the performance and scalability of the traditional silicon-based devices.[1, 19] Nonetheless, some remarkable differences should be noted between C and Si/Ge based nanosheets. The buckled honeycomb structure of silicene and germanene leads to a significantly larger chemical reactivity than graphene, and thus, to a much stronger trend for adsorption of atoms and molecules.[1, 19, 20] In silicene / germanene sheet, silicon / germanium owns sp^3 hybridization, which is the most favorable configuration in comparison with the sp^2 or the mixed sp^2-sp^3 orbitals. This sp^3 hybridization leads to common covalent Si-Si / Ge-Ge bonds in a low buckled structure.[1, 19, 21] 2D heterostructures such as boron nitride (BN) are composed of equal number of alternating boron and nitrogen atoms with sp^2 hybridization in a honeycomb arrangement, with similar structure than graphene. BN sheets are intrinsically insulators (or wide gap semiconductors), stable up to 1000 K and more resistant to oxidation than graphene.[22] All these properties justify the great interest on Si, Ge and BN nanosheetst. As for graphene, properties of different Si, Ge and BN sheets can be tuned through the adsorption of different molecules. This has led to several works in the last years dealing with the surface functionalization of Si,[1,18, 19, 23-25] Ge[1, 19, 20] or BN[1,22, 26-29] nanosheets. These studies point out that new hybrid system based on hexagonal nanosheets with concrete features could be designed through the adsorption of adequate molecules on the surface. In spite of the wide interest on 2D surface functionalization through molecular adsorption, there is still scarce information about the absorption of different molecules on silicene, germanene and BN sheets. Experimental techniques, such as Atomic Force microscopy, scanning tunneling microscopy or X-Ray spectroscopy, as well as theoretical method like ab initio quantum chemistry methods (mainly Density Functional Theory, DFT), molecular dynamics (MD) and Monte Carlo (MC) simulations have been applied to study ionic-liquid graphene interface.[8, 10, 11, 15, 16, 17] As previously noted, those works, are mainly limited to classic ILs. Some works about ILs on BN nanosheets have been also reported,[29, 30] while studies on IL on silicene or germane surfaces have been not published.

Although DFT simulations are limited to relatively simple theoretical models, they have been proven their ability in providing useful information for the design of functionalizated nanosheets.[6-8] In addition, DFT methods allow a deeper knowledge of interaction of ILs at the

surface, explaining their electronic structure and shedding light on the interaction mechanism. Therefore, a DFT study on the adsorption of ILs on C, Si, Ge and BN based hexagonal nanosheets is reported in this work. Concretely, the adsorption Choline Benzonate ([CH][BE], Figure 1) ionic liquid was here studied. Choline ([CH]) based ionic liquids are a new family of ionic liquids[31] with suitable properties such as null toxicity, high biodegradability or low cost. Likewise, the combination of choline cation with benzoate anion ([BE]) leads to an ionic liquid composed totally of biomaterials,[32] which can be produced at very low cost,[33] and with null environmental impact. Thus, [CH][BE] ionic liquid has been selected in this work as a first example in the study of the adsorption of ILs on different nanosheets.

2. THEORETICAL METHODOLOGY

DFT simulations were carried out using the generalized gradient approximation of Perdew, Burke and Ernzerhof (PBE)[34] as implemented in the SIESTA 3.2 package,[35] along norm-conserving Troullier-Martins pseudopotentials[36] and numerical double-ζ polarized (DZP) basis sets. All calculations were done with an energy mesh cut-off of 400 Ry and a k-point mesh of 8 × 8 × 8 in the Monkhorst-Pack scheme.[37] Model nanosheets were described as a 2D honeycomb structure of 128 atoms with periodic boundary conditions (PBC) applied in the three space directions. PBC in the direction normal to the nanosheet surface was 30 Å, long enough to avoid interaction between image layers. Structural relaxation were done by conjugate gradients, with convergence criteria being forces acting on all atoms do not exceed 0.03 eV/Å.

PBE functional has been successfully applied to study interaction between different molecules and C,[38, 39] Si,[24, 40] Ge[41] or BN[22, 28] nanosheets. Long range dispersion interactions are expected to be important for an adequate description of IL-nanosheet systems under study. In this sense, it is well known that the most common GGA (Generalized Gradient Approximation) functionals show shortcomings for the adequate description of long range dispersion interactions.[42] Even though, some reported results have shown that dispersion corrections are not required in some cases for which molecules develop van der Waals interactions.[7, 39] On the other hand, many studies have pointed out the need of adequate description of dispersive interactions.[7, 20, 25, 26, 43] Therefore, dispersion corrections, according to Grimme's scheme,[44] over PBE functional (PBE-D2) were also employed to obtain information about the effect of dispersion corrections on calculated properties.

[CH][BE]-nanosheet models were built (randomly) placing the optimized geometry of the ionic liquid onto the nanosheet. In this starting geometry, the IL was placed to allow a π-

stacking interaction between the phenyl motif and the surface with a distance of around 3.5 Å (typical π-stacking interaction). These starting geometries were optimized. Then, the relative disposition (through longitudinal displacements) over the surface, as well as the rotational angle through the main bond between both ions (see d_1, Figure 1) holding the above mentioned π-stacking between phenyl motif and the surface have been assessed. These analyses were carried out based on previously optimized geometries through single pointscalculations. From previous single points, choline benzonate ionic liquid was placed at the most stable disposition over each nanosheet and these [CH][BE]-nanosheet models were optimized, which leaded to the optimized structures here discussed.

Binding energies, *BE*, between [CH][BE] and the corresponding nanosheets were estimated as:

$$BE_{IL\text{-}S} = (E_S + E_{IL}) - E_{IL\text{-}S} \quad (1)$$

where E_S, E_{IL}, and $E_{IL\text{-}S}$ stand for the total energy of the sheet, ionic pair and total energy of the IL-nanosheet, respectively. *BE* corresponding to the interaction between ions was defined as:

$$BE_{IL} = (E_{cat} + E_{ani}) - E_{IL} \quad (2)$$

where E_{cat} and E_{ani} are the total energy of the cation and the anion, respectively. Charge transfer (CT) between graphene and IL has been studied through Hirshfeld[45] and ChelpG[46] atomic charges. ChelpG scheme has proven to be adequate for describing atomic charges in ILs,[47, 48] while Hirshfeld model is an alternative definition of atomic charges based on partitioning of the electron density.[45] Interactions between IL and the nanosheets were featured through both a topological analysis of the electron density, according Bader's[49] theory (Atoms in Molecules, AIM), and the analysis of the reduced density gradient (RGD) at low densities.[50] According to AIM theory,[49] there are four kinds of critical points, but because of the characteristics of the studied systems, and for improving and clarifying data analysis, attention has been paid to bond critical points (BCP), which rises the criteria for considering the presence of intermolecular interactions, through the computed electronic density (ρ) and its laplacian ($\nabla^2\rho$). Nevertheless, some information regarding to the adsorption process could be also obtained from ring and cage critical points (RCP and CCP, respectively). RGD analysis is able to find non-covalent interactions based on the peaks that appear at low densities. Thus, the visualization of RGD iso-surfaces for these peaks allows the localization of weak interactions. The strength and nature of the interactions is determined through the sign of the second density Hessian eigenvalue.[50] AIM and RGD analysis were carried out

using MultiWFN code.[51] Partial density of States (PDOS) were extracted with the program developed by A. Postnikov.[52]

3. RESULTS AND DISCUSION

3.1 Choline Benzonate on nanosheets. Figure 1 shows the optimized structure of isolated [CH][BE] ionic pair. As seen, there are several intermolecular interactions between both ions, labeled as d_1-d_4. All these interactions are hydrogen bonds, where oxygen atoms of carboxyl group in the benzoate anion play as hydrogen bond acceptor. As seen in Table 1, both intermolecular distances and AIM parameters (BCP associated with these intermolecular interactions) are only slightly affected by the use of dispersive corrections (PBE-D2 functional). Intermolecular hydrogen bond between hydroxyl group of choline cation and COO- group of benzoate anion (d_1) the strongest one. This hydrogen bond yields a distance equal to 1.673 Å and ρ = 0.0668 a.u. (at PBE/DZP level), which are similar for those previously described for [CH[BE] ionic liquid.[48] Despite the presence of intermolecular hydrogen bonds, it is well known that cation-anion interactions in ionic liquids are mainly governed by coulombic forces. In addition, there is a remarkable charge transfer of 0.69/0.50 e^- (estimated through ChelpG/Hirshfeld at PBE/DZP level).

The most stable configurations of IL-nanosheet systems along with their calculated properties are reported in Figures 2-5 and Tables 2-5. Following the labeling used in Figure 1, intermolecular interactions between both ions are labeled as d_1-d_4. Regarding to [CH][BE] on top of the graphene sheet, intermolecular interactions d_1-d_4 are not dramatically affected upon adsorption process. For example, in average bond variation after the adsorption process is equal to 0.026 Å / 0.070 Å using PBE/PBE-D2 functional. These small bond small variations point out that the main features of the ionic liquid are also present for the ionic liquid on top of the nanosheet. Similar trend was found for atomic charges, which are similar to those ones estimated in absence of graphene surface. At PBE-D2/DZP level and using ChelpG scheme, cation/anion loses its positive/negative charge (0.07/0.13 e^-), while graphene surface has a charge of -0.06 e^-. The negative sing of graphene charge indicates a small charge transfer from the ionic liquid (concretely from the anion) to the surface. The remaining anionic lost charge stands for the increase noted on the cationic charge. Thus the adsorption of IL on graphene leads to a charge transfer between ions of 0.34 e^- according ChelpG scheme at PBE/DZP level. In general terms, similar conclusions are obtained for the interaction between both ions in presence of boron-nitride sheet. Even though, Hirshfeld model predicts a higher charge transfer between the anion and BN based surface (0.26 e^-).

The adsorption of choline benzoate on silicene leads to a proton transfer between both ions (Figure 3). As can be seen in Table 3, d_1 = 1.026 Å at PBE/DZP level, which is a typical O-H bond length, in agreement with its high electronic density value and negative laplacian. d_0 distance has been defined as the bond between both O and H atoms corresponding to hydroxyl choline motif (Figure 3). This distance (d_0) yields features corresponding to an intermolecular hydrogen bond, such a d_1 for the isolated ILs. All these factors points out a clear proton transfer from the cation to the anion. ChelpG/Hirshfeld yield an interionic CT = 0.37 e^-/ 0.28 e^-, whereas charge transfer from the anion to the silicene is 0.06 e^-/ 0.54 e^-. Hirshfeld atomic charges lead to a greater charge transfer up to the surface with the consequent negative charge reduction over the benzonate, while there is a decrease for the inter-ionic CT. PBE-D2 functional also predicts a proton transfer between both ions. However, there is a strengthening for d_0 interaction (which decreases / increase its length/ electronic density) in comparison with optimized structure at PBE level. Both ChelpG and Hirshfeld models yield smaller inter-ionic CT (of around 0.30 e^-) than isolated IL, while CT to the silicene surface increases up to 0.65 e^-.

Optimized structure of [CH][BE] on Ge based surface at PBE/DZP level is showed in Figure 4. As can be seen in Table 4, d_1 suffers a shortening (0.261 Å) along to an electronic density increase due to the adsorption process, which results in a strengthening of the interaction between both ions. In addition, the relative disposition of choline hinders the interaction d_4 (the corresponding BCP was not found). According with Hirshfeld model, cation/anion charge becomes more positive / less negative, whereby interionic CT decreases 0.19 e^-, while there is an important CT from the anion up to the germanene (CT = 0.54 e^-). The use of dispersions corrections in PBE functional (PBE-D2) leads to a proton charge transfer from the cation to the anions (d_0 and d_1 bond lengths and AIM parameters computed at PBE-D2/DZP level in Table 4).

In short, the most dramatic changes upon adsorption process are the proton transfer for IL-Si system (also for IL-Ge at PBE-D2/DZP level), and CT computed according to Hirshfeld model. Isolated choline benzonate, IL-graphene and IL-BN systems,yield an inter-ionic CT $\simeq$ 0.50 e^-, while this CT is equal to 0.28 e^- /0.19 e^- for the IL on silicene / germanene surface (at PBE/DZP level). In addition, due to the adsorption process, the new arrangement between both ions leads to a new cage critical point (labeled as CCP1, Figures 2-5 and Tables 2-5), whose ρ could provide some information on interionic interaction strength. This CCP yields similar ρ values for [CH][BE] on top of C, Si and BN sheets, while the largest ρ values are obtained for IL on top of germanene.

3. 2 Adsorption Mechanism:[CH][BE]-nanosheet interactions. As concerns as the changes on the structure of studied nanosheets upon the adsorption process, Δd_{X-X} parameter (see Tables 2-5) has been defined as the difference value of X-X after and before of the adsorption process (X-X = C-C, Si-Si, Ge-Ge or B-N) bonds corresponding to nanosheets after and before of the adsorption process. Despite the studied IL-nanosheets systems and the theoretical level (without dispersion corrections or dispersion corrected functional), $\Delta d_{X-X} \leq$ 0.009 Å, which points out that the nanosheet structure does not suffers important change upon the ionic liquid adsorption. In addition, graphene and boron-nitride sheets keep their planarity after the adsorption process, while silice and germanene sheets also maintain their buckled structure.

Results reported in Figures 2-5 show that the phenyl (benzoate) motif adopts a configuration parallel to the surface. The average interplanar distances between phenyl moiety and different sheets (labeled as d_{eq}, Tables 2-5) were found to be of roughly 3.65 Å for IL-graphene and IL-silecene systems and $\simeq$ 3.74 Å for IL-germanene and IL-boron nitride at PBE/DZP level. For [CH][BE] on graphene sheet, d_{eq} computed at PBE/DZP level lies close to the typical π-stacking distance (3.5 Å - 4.0 Å). However, PBE-D2/DZP level brings an approach ($\simeq$ 0.50 Å) between both planes.

The adsorption of phenyl motif on graphene sets up three interactions with the surface (d_5-d_7), whose average distance is 3.625Å (at PBE/DZP level). Besides, carboxylate group also develops a link with the surface (d_8). The dihedral angle between phenyl and carboxylate motifs (τ_1) is 0.0 degrees, which hinders an approach between the carboxylate group (which keeps most of the negative charge) and the surface. Hence, the CT (0.02 e^- according Hirshfeld scheme at PBE/DZP level) from the anion up to graphene sheets is close to zero. Silicene/Germanene surfaces establishes 3/2 intermolecular bonds with the phenyl motifs (labeled as d_5-d_7 /d_5, d_6), whose distances are larger than those ones found for IL-graphene system (Figures 3,4 and Tables 3,4). Nonetheless, all of them yield larger electronic density values, which would point out to stronger interactions between phenyl motif and the surface. Due to the larger diameters for those rings forming the Si/Ge surface, bonds between the surface and the phenyl are not perpendicular to the surface plane. In this case, τ_1 = 15.3 degrees / 16.7 degrees, which allows a shortening of the distance between carboxylate group and the surface. Two / one interactions were found between the carboxylate group and the Si/Ge sheet (d_8, d_9 / d_7). The CT (0.54 e^- /0.68 e^- according Hirshfeld scheme at PBE/DZP level) between the anion and the germanene surface agrees with the shortest distance between the carboxyl group and the surface (2.318 Å at PBE/DZP level). Likewise, benzoate anion is

able to develop five interactions with the boron-nitride surface (Figure 5), four of them through phenyl motif (d_5-d_8) and the other one through COO^- group (d_9). For [CH][BE] of top of BN sheet, τ_1 is close to the planarity. This dihedral angle obstructs an approach (d_9 = 3.900 Å at PBE/DZP level) between COO^- group of benzoate and the BN surface, leading to small CT from the anion to the BN sheet (0.11 e^- according Hirshfeld scheme at PBE/DZP level).

[CH]-surface interactions are always carried out through two intermolecular bonds between the oxygen atom and methylene group with the surface. Moreover, germanene sheet allows another additional interaction with the methylene group (see Figure 4). The shortest distance between [CH] and the surface is found for IL-silicene system (d_{10} = 1.841 Å at PBE/DZP level, Table 3). The presence of choline benzonate on silicene surface brings a deformation of silicene sheet, which allows a shorter length for d_{10} (d_{10} = 1.841 Å for IL-Si/ system at PBE/DZP). Different behavior is found regarding to the interaction strength (based on distance and electronic density values) between the oxygen atom and methylene group with the surface (d_{10} = 2.762 Å / d_{11} = 2.867 Å / d_9 = 3.032 Å and d_{10} = 3.056 Å /d_{11} = 2.66 Å for IL-C / IL-Si /IL-Ge / IL-BN systems at PBE/DZP).

In addition to the information related with intermolecular IL-sheet interactions (labeled as d_5-d_{11}) and the AIM properties for their corresponding BCP, main AIM parameters for RCPs and CCPs (red and purple points in Figures 2-5) have been also collected. Aimed at looking for a relationship between the interaction strength for IL-nanosheet systems and AIM parameters, the total value of electronic density of the different calculated critical points is also gathered in Tables 2-5. Some relationships were found between AIM parameters for intermolecular interaction and binding energies. For example, Si and Ge based surfaces provides the largest value for the total electronic density for those BCPs related with the interactions between the ionic liquid and the surface ($\sum$(BCP)). Silicene and germanene sheets allow stronger interactions than graphene or boron-nitride surfaces.

As seen for d_{eq}, PBE-D2 functional estimates, in general, shorter intermolecular distances between the IL and the surfaces, which leads to an increase of some factors related with the intermolecular interactions, such as interaction strength (based on electronic density value) and IL-surface charge transfer.

The nature of the interaction between [CH][BE] ionic liquid and different nanosheets was elucidated based on RGD iso-surfaces. For [CH][BE]-nanosheet systems, the RGD iso-surfaces are displayed in Figures 2-5. The green color for the regions between the IL and the nanosheets points out that van der Waals interactions are the main force responsible for the IL adsorption on nanosheets regardless the considered nanosheet. The largest iso-surface

between phenyl motif and BN surface is in concordance with the parallel disposition between both phenyl motif and BN sheet. In short, anion-surface interactions should be the main contribution to the IL-surface binding energies.

As mentioned in previous sections, the available literature dealing with the adsorption of IL on nanosheets is very scarce (mainly limited to imidazol based ILs on graphene). Recently, Herrera *et al.* previously studied the adsorption of imidazol cation pared amino acid based anion graphene surface,[8] while Shakourinan-Fard *et al.* analyzed IL adsorption on BN nanosheets for classical ILs,[29] both of them through DFT methods. The first employed PBE-D2/DZP, while a meta-GGA functional was selected for the later. Both approximations should provide a good description for the dispersion forces.[44, 53] However, despite the IL (choline benzoate, aminoacid based or classical ILs), the surface (graphene or boron-nitride) or the applied methods (DFT-D2 or meta-GGA), similar structural features were inferred, *i.e.,* IL-surface distances of around 3.0 Å were found, being IL-surface interactions mainly featured by π-stacking interactions between aromatic ions (imidazol cation for previously reported works or benzoate anion in this paper) and the surface.

3.3 Binding Energies. Main intermolecular interactions between both ions as well as between the ionic liquid and the nanosheets were analyzed in previous sections. In addition, binding energies can be used as a measurement of the interaction strength. Binding energies of the interaction between both ions (BE_{IL}, Figure 6) was 84.31kcal mol^{-1} at PBE/DZP level. This high value is mainly due to the important contribution from the coulombic forces between both ions. Figure 6 also gathers BE_{IL} of the IL on top of the nanosheets, which were calculated from the previously optimized IL geometry on top of each nanosheets. As seen in Figure 6, BE_{IL} decreases from IL on top of graphene up to IL on top of germanene, while [CH][BE] on top of BN yields larger BE_{IL}. IL adsorption on graphene, silicon or germane brings a BE_{IL} up to 16.34 kcal mol^{-1}, while choline benzoate on top of boron-nitride yields BE_{IL} 83.94 kcal mol^{-1}. Hence, the adsorption of choline benzoate on the studied homo nanosheets has important drawbacks on BE_{IL}. Albeit there is an important proton transfer from choline up to benzoate for IL-silicene systems, this fact would have not important effects on the interaction between both ions on silicene surface. BE_{IL} at PBE-D2/DZP level (which are somewhat larger, mainly due to smaller intermolecular distances) follow a similar pattern upon adsorption process. Coulombic forces between ions play an importance role in the interionic interactions. In fact, [CH][BE] on silicene and germanene provides the lowest interionic CT and the lowest BE_{IL}. As said, intermolecular interactions (such as hydrogen bonds) are also an

important contribution to BE_{IL}. In this sense, Figure 6 also displays dispersion energy contribution ($BE_{dis,IL}$) to the total binding energy (quantified according to Grimme's approach[44] for PBE-D2 functional). $BE_{dis,IL}$, which is very close to the difference between the binding energy between both (dispersion) corrected and not corrected functionals, only stands a small contribution to the total BE_{IL}, Figure 6.

Figure 7 collects binding energies for the interaction between the ionic liquid and different nanosheets *(BE_{IL-S})*. At PBE/DZP level BE_{IL-S} follows as: graphene $\simeq$ boron-nitride < germanene < silicene. The adsorption [CH][BE] on top of graphene and boron-nitride yields $BE_{IL-S} \simeq$ 12.24 kcal mol^{-1}, while those values increase up to 19.41 kcal mol^{-1} and 34.49 kcal mol^{-1} for Ge and Si based sheets, respectively. As previously noted, interactions between choline benzoate and silicene lead to a surface distortion, which allows a short intermolecular distance between the cation and the surface (d_8, see Figure 3). However, this effect is not displayed in IL-germanene system. At PBE-D2/DZP level, computed BE_{IL-S} values follow similar pattern, however both IL-silicene and IL-germanene systems yield similar BE_{IL-S} ($\simeq$ 49.65 kcal mol^{-1}). Figure 7 also draws the contribution from $BE_{dis,IL-S}$ to the total BE_{IL-S} estimated using PBE-D2 functional. Note that $BE_{dis,IL-S} \simeq$ 28.67 kcal mol^{-1}, except for IL-germanene systems, whose $BE_{dis,IL-S}$ = 39.43 kcal mol^{-1}. As seen in Tables 2-5, most intermolecular IL-Germanence distances are, in general, shorter than those obtained for the remaining systems, which would lead to an enhancement of the dispersion contribution. These high $BE_{dis,IL-S}$ values prove that dispersion interactions are the main driving force between selected IL and surfaces. Those results agree with iso-surfaces features previously described. In general, the highest values obtained for IL-silicene and IL-germanene systems would be due to their buckled honeycomb structure, which allow a higher chemical reactivity than graphene, leading to a much stronger adsorption of atoms and molecules.[1, 19, 20]

Previously reported work estimated that BE_{IL-S} for different ionic liquid on top of graphene[8] or boron-nitride[29] sheets were roughly 63.00 kcal mol^{-1} (at PBE-D2/DZP level) and 19.74 kcal mol^{-1} (PBE-D3/TZP) , respectively. In these works, nanosheets mainly main tends to interact with cation. However in this work, the larger contribution to the BE_{IL-S} comes from anion-sheet interactions.

3.4 Electronic Structure. Figure 8 shows the density of states (DOS) for [CH][BE] and [CH][BE]-nanosheet systems at PBE/DZP (although similar results can be drawn with PBE-D2 functional). DOS for pristine nanosheets, partial density of states corresponding to the [CH][BE] ionic liquids, as well as the contributions from both ions are also reported in Figure

8. There are several works dealing with the electronic structure of pristine nanosheets,[1, 18, 19, 40, 54] and the results reported in Figure 8 are in agreement with available data, which show zero gap semiconductor characteristic for all cases, except for boron-nitride nanosheets which show insulator character (wide gap). The adsorption of choline benzoate ionic liquid on graphene, silicene or germanene has not a dramatic effect on the nanosheet electronic structure, Figure 8, with only both valence /conductivity bands slightly increasing their energies (~ 0.20 eV). For IL on silicene and germane, the highest / lowest occupied/unoccupied orbitals corresponding to the ionic liquid (i.e. HOMO and LUMO over ionic liquid motif) are far from the valence and conduction band of the IL-nanosheets systems. The same features are also noted for LUMO orbital over IL for IL-graphene systems, while HOMO orbital is closer in energy to the valence band. Therefore, IL adsorption does not change its zero gap character. As regards as boron-nitride nanosheet, IL presence leads to a decrease of its band gap, from 3.93 eV up to 3.45 eV (at PBE/DZP level). After the adsorption process, the highest occupied level is due to the IL, which is higher in energy that the boron-nitride valence band. In addition, interaction with the IL leads to a conductivity band destabilization, which yields energies near to the LUMO.

From PDOS plotted in Figure 8 information about cation and anion contributions to their corresponding HOMO and LUMO orbitals is inferred. The same information is easily obtained from the molecular orbital contours reported in Figure 9. The LUMO of the isolated ionic liquid is mainly localized over the benzoate anion. The same behavior is also found for [CH][BE] on top of the selected nanosheets. The adsorption on graphene / boron-nitride nanosheets brings a LUMO energy decrease of 0.36 eV / 0.48 eV, while the adsorption on silicene / germanene leads to a LUMO energy diminution $\simeq$ 1.71 eV(at PBE/DZP level). Similar patterns are obtained for the HOMO energies, *i.e.* the adsorption on graphene, boron-nitride or silicene/germanene leads to a HOMO energy diminution equal to 0.32 eV, 0.44 eV or 2.32 eV. Hence, isolated ionic liquid as well as ionic liquid on top of graphene or boron-nitride surfaces yield a HOMO-LUMO difference of around 3.46 eV; while the larger HOMO energy change for choline benzoate on top of silicene or germanene provides a HOMO-LUMO difference $\simeq$ 4.07 eV (at PBE/DZP level). However, the contribution from each ion to the HOMO orbital varies as a nanosheet function. HOMO orbital is located over the choline motif, although it also shows a very important contribution from the benzoate anion, for isolated [CH][BE] and choline benzonate on top of graphene / boron-nitride sheet. For these systems, interionic CT $\simeq$ 0.32 e^- / 0.51 e^- (according ChelpG / Hirshfeld models); while CT from benzoate to sheet is close to zero (for both ChelpG / Hirshfeld schemes) at PBE/DZP

theoretical level. For the ionic liquid on top of silicene or germane sheets, interionic CT $\simeq$ 0.28 e^- or 0.19 e^-, respectively, according Hirshfeld populations. Both IL-silicene and IL-germanene systems yield an important CT from the ionic liquid (concretely from the anion) to sheet, equal to 0.54 e^- and 0.68 e^- respectively. These high CT values lead to the HOMO orbital being mainly located on the benzoate anion. In addition, these HOMO contours also show some similarities with the HOMO-1 orbital for the pristine ionic liquid. IL-nanosheet CTs according to ChelpG model are close to zero. There should be a relationship between the IL-sheet CT transfer according to Hirshfeld method and the HOMO energy: the greater / smallest CT is obtained for those nanosheets which are able to provide the lowest / highest HOMO (from the ionic liquid) energy. Therefore, Hirshfeld could be more appropriate to study the adsorption on IL on top of nanosheets.

4. CONCLUSIONS

The adsorption of choline benzoate ionic liquid on the surface of 2D nanosheets, graphene, silicene, germanene and boron-nitride, was studied using DFT approach. The interaction mechanisms, binding energies and electronic structure were calculated using the PBE functional as well as PBE plus dispersion corrections (PBE-D2). The latter has provided useful information on the contributions from dispersion forces to the interaction between both ions (which is mainly due to coulombic forces) as well as the interaction between the IL and the nanosheet, which is mainly due to dispersion forces. Even though charge transfer from the anion to the surface also plays an important role. There is also a relationship between interionic interaction and ionic liquid - nanosheet ones. Therefore, the larger interionic binding energies are obtained for choline benzoate on top of carbon and boron nitride based sheets, which provides the lowest IL-sheet interaction energies. The analysis of results has showed that the considered sheets interact with the anion through π-stacking, although there is also a remarkable charge transfer for IL-silicene and IL-germanene. The electronic structure analysis exposed that nanosheet electronic structure is not affected upon IL adsorption process. However, HOMO and LUMO molecular orbitals located on the IL suffer changes in their energies upon adsorption. Thus, the largest changes are noted for choline benzoate on top of silicene and germanene sheets. For both systems, there is also a larger charge transfer from the IL to the sheet, which leads to changes on the molecular fragment contributions to the HOMO contours. In this work, ChelpG and Hirshfeld models have been used to compute charge transfer processes, with results showing that only Hirshfeld method would provide coherent values for IL-sheet charge transfer processes and their relationship with binding

energies or with the molecular orbital shapes. In short, IL-graphene and IL-BN would provide similar features (such as interaction mechanism, CT, binding energies or electronic structure), while IL-silicene and IL-germanene would bring greater changes on assessed properties.

The reported results provide useful information on the ionic liquid absorption for different nanosheets and their interaction mechanisms. They could be also considered as a insight up for the tuning of ionic liquid properties through the adsorption on the adequate nanosheet.

ACKNOWLEDGEMENT

This work was made possible by Ministerio de Economía y Competitividad (Spain, project CTQ2013-40476-R) and Junta de Castilla y León (Spain, project BU324U14). Gregorio García acknowledges the funding by Junta de Castilla y León, cofounded by European Social Fund, for a postdoctoral contract. We also acknowledge The Foundation of Supercomputing Center of Castile and León (FCSCL, Spain), Computing and Advanced Technologies Foundation of Extremadura (CénitS, LUSITANIA Supercomputer, Spain), and Consortium of Scientific and Academic Services of Cataluña (CSUC, Spain) for providing supercomputing facilities. We also thank Dr. S. Cahangirov and S. Ciraci (Bilkent Unversity) for providing us the structures for pristine graphene, silicene and germanene nanosheets. The statements made herein are solely the responsibility of the authors.

REFERENCES

1. M. Xu, T. Liang, M. Shi, H. Chen, *Chem. Rev.,* 2013, **113**, 3766-3798.
2. H. Y. Mao, S. Laurent, S. Chen, W. O. Akhavan, M. Imani, A. A. Ashkarran, M. Mahmoudi, *Chem. Rev.,* 2013, **113**, 3407-3424.
3. K. S. Novoselov, A. K. Geim, S. V. Morozov, D. Jiang, Y. Zhang, S. V. Dubonos, I. V. Grigorieva, A. A. Firsov, *Science* 2004, **306**, 666-669.
4. J. K. Wassei, R. B. Kaner, *Acc. Chem. Res.,* 2013, **46**, 2244-2253.
5. X. Hu, Q.Zhou, *Chem. Rev.,* 2013, 113, 3815-3835.
6. V. Georgakilas, M. Otyepka, A. B. Bourlinos, V. Chandra, N. Kim, K. C. Kemp, P. Hobza, R. Zboril, K. S. Kim, *Chem. Rev.,* 2012, **112**, 6156-6214.
7. J. Björk, F. Hanke, C. A. Palma, P. Samori, M. Cecchini, M. Persson, *J. Phys. Chem. Lett.,* 2010, **1**, 3407-3412.
8. C. Herrera, R. Alcalde, M. Atilhan, S. Aparicio, *J. Phys. Chem. C,* 2014, **118**, 9741-9757.
9. M. Sha, M. Wu, G. Y. Liu, Z. Tang, H. Fang, *J. Phys. Chem. C,* 2009, **113**, 4618-4622 T. Fukushima, T.Aida, *Chemistry,* **2007**, 13, 5048-5058; Y. Shim, Y. Jung, H. J. Kim, *J. Phys. Chem. C,* 2011, **115**, 23574-23583.
10. S. Aparicio, M. Atilhan, *J. Phys. Chem. C,* 2012, **116**, 12055-12065.
11. A. S. Pensado, F. Malberg, M. F. C. Gomes, A. A. H. Padua, J. Fernandez, B. Kirchner, *RSC Advances,* 2014, **4**, 18017-18024.
12. M. Tunckol, J. Durand, P. Serp, *Carbon* 2012, **50**, 4303-4334.
13. S. Aparicio, M. Atilhan, F. Karadas, F., *Ind. Eng. Chem. Res.,* 2010, **49**, 9580-9595 J. S.Wilkes, *Green Chemistry,* 2002, **4**, 73-80 J. Earle-Martyn, R. Seddon-Kenneth, Ionic Liquids: Green Solvents for the Future. In *Clean Solvents*, American Chemical Society. **2002**.

14. N. V. Plechkova, K. R.Seddon, *Chem. Soc. Rev.,* 2008, **37**, 123-150 Z. Lei, C. Dai, B. Chen, *Chem. Rev.,* 2013, **114**, 1289-1326.
15. H. Zhou, M. Rouha, G. Feng, S. S. Lee, H. Docherty, P. Fenter, P. T. Cummings, P. F. Fulvio, S. Dai, J. McDonough, V. Presser, Y. Gogotsi, *ACS Nano* 2012, **6**, 9818-9827 Q. Dou, M. L. Sha, H. Y. Fu, g. Z. Wu, *J. Phys.: Condens. Matter,* 2011, **23**, 175001.
16. M. H.;Ghatee, F. Moosavi, *J. Phys. Chem. C,* 2011, **115**, 5626-5636; T.;Carstens, R.;Gustus, O.;Höfft, N.;Borisenko, F.;Endres, H.;Li, R. J.;Wood, A. J.;Page, R. Atkin, *J. Phys. Chem. C,* 2014, **118**, 10833-10843; A. J. Page, A. Elbourne, R. Stefanovic, M. A. Addicoat, G. G. Warr, G. G. Voitchovsky, K. R. Atkin, *Nanoscale* 2014, **6**, 8100-8106; M.;Vijayakumar, B.; Schwenzer, V.;Shutthanandan, J.;Hu, J.;Liu, I. A Aksay, *Nano Energy,* 2014, **3**, 152-158; S. A.;Kislenko, I. S.;Samoylov, R. H. Amirov, *Phys. Chem. Chem. Phys.,* 2009, **11**, 5584-5590.
17. G.;Kamath, G. A. Baker, *Phys. Chem. Chem. Phys.,* 2012, **14**, 7929-7933; D.;Wagle, G.;Kamath, G. A. Baker, *J. Phys. Chem. C,* 2013, **117**, 4521-4532; S.;Ravula, S. N.;Baker, G.;Kamath, G. A. Baker, *Nanoscale,* 2015, **7**, 4338-4353.
18. D. Jose, A. Datta, *Acc. Chem. Res.,*2013, **47**, 593-602.
19. A. Kara, H. Enriquez, A. P. Seitsonen, L. C. Lew Yan Voon, S. Vizzini, B. Aufray, H. Oughaddou, *Surface Science Reports* 2012, **67**, 1-18.
20. W. Xia, W. Hu, Z. Li, J. Yang, *Phys. Chem. Chem. Phys.,* 2014, **16**, 22495-22498.
21. S. Wang, *Phys. Chem. Chem. Phys.,* 2011, **13**, 11929-11938.
22. Y. Tian, X.F. Pan, Y.J. Liu, J.X.Zhao, *Applied Surface Science* 2014, **295**, 137-143.
23. N. J. Roome, J. D. Carey, *ACS Applied Materials & Interfaces* 2014, **6**, 7743-7750 N. Gao, W. T. Zheng, Q. Jiang, *Phys. Chem. Chem. Phys.,* 2012, **14**, 257-261. R.;Wang, X.;Pi, Z.;Ni, Y.;Liu, D. Yang, *RSC Advances,* 2015, **5**, 33831-33837; B.;Huang, H. J.;Xiang, S.-H. Wei, *Phys. Rev. Lett.,* 2013, **111**, 145502.
24. T. H. Osborn, A. A. Farajian, O. V. Pupysheva, R. S. Aga, L. C. Lew Yan Voon, *Chemical Physics Letters* 2011, **511**, 101-105.
25. W. Hu, N. Xia, X. Wu, Z. Li, J. Yang, *Phys. Chem. Chem. Phys.,* 2014, **16**, 6957-6962 T. P. Kaloni, G. Schreckenbach, M. S. Freund, *J. Phys. Chem. C,* 2014, **118**, 23361-23367.
26. N.;Ding, N.; X.;Chen, Wu, L.;C.-M. H. Li, *Phys. Chem. Chem. Phys.,* 2013, **15**, 10767-10776.
27. H.;Liu, C. H.Turner, *Phys. Chem. Chem. Phys.,* 2014, **16**, 22853-22860.
28. S. L.;Tang, Y. J.Liu,; H. X.;Wang, J. X.;Zhao, Q. H.;Cai, X. Z.Wang, *Diamond and Related Materials,* 2014, **44**, 54-61.
29. M. Shakourian-Fard, G. Kamath, Z. Jamshidi, *J. Phys. Chem. C,* 2014, **118**, 26003-26016.
30. G. Kamath, G. A. Baker, *RSC Advances,* 2013, **3**, 8197-8202.
31. D. J. Couling, R. J. Bernot, K. M. Docherty, J. K. Dixon, E. J. Maginn, *Green Chemistry,* 2006, **8**, 82-90.
32. M. Petkovic, J. L. Ferguson, H. Q. N. Gunaratne, R. Ferreira, M. C. Leitao, K. R. Seddon, L. P. N. Rebelo, C. S. Pereira, *Green Chemistry,* 2010, **12**, 643-649.
33. Y Y. u, X. Lu, Q. Zhou, K. Dong, H. Yao, S. Zhang, *Chemistry,* 2008, **14**, 11174-11182.
34. J. P. Perdew, K. Burke, M. Ernzerhof, *Phys. rev. Lett.,* 1996, **77**, 3865.
35. J. M. Soler, E. Artacho, E. Gale, J. D. A. García, J. Junquera, P. Ordejón, D. Sánchez-Portal, *J. Phys.: Condens. Matter,* 2002, **14**, 2745.
36. N. Troullier, J. L. Martins, *Phys. Rev. B.,* 1991, **43**, 1993-2006.
37. H. J. Monkhorst, J. D. Pack, *Phys. Rev. B.,* 1976, **13**, 5188-5192.
38. J. G. Hernández, E. Anota, M. R. de la Cruz, M. Melchor, G. Cocoletzi, *J. Mol. Mod.*, 2012, **18**, 3857-3866 R. R. Q. Freitas, R. R. Q. Rivelino, R. F. D. B. Mota, C. M. C. de Castilho, *J. Phys. Chem. A,* 2011, **115**, 12348-12356 T. Hu, I. C. Gerber, *J. Phys. Chem. C,* 2013, **117** , 2411-2420.
39. Lechner, A. F. Sax, *J. Phys. Chem. C,* 2014, **118**, 20970-20981.
40. J. W. Feng, Y. J. Liu, H. X. Wang, J. X. Zhao, Q. H. Cai, X. Z. Wang, *Comp. Mater. Sci.*, 2014, **87**, 218-226.
41. Y. Ma, Y. Dai, C. Niu, B. Huang, *J. Mater. Chem.,* 2012, **22**, 12587-12591.
42. A. J. Cohen, P. Mori-Sánchez, W. Yang, *Chem. Rev.,* 2012, **112**, 289-320.
43. Q.;Sun, Z.;Li, D. J.;Searles, Y.;Chen, G.;Lu, A. Du, *J. Am. Chem. Soc.,* 2013, **135**, 8246-8253.
44. S. Grimme, *J. Comput. Chem.,* 2006, **27**, 1787-1799.
45. F. L. Hirshfeld, *Theor. Chim. Acta,* 1977, **44**, 129-138.
46. C. M. Breneman, K. B. Wiberg, *J. Comput. Chem.,* 1990, **11**, 361-373.
47. S. Aparicio, M. Atilhan, *Chem. Phys.* 2012, **400**, 118-; S. Aparicio, M. Atilhan, *Energy Fuels* 2013, **27**, 2515-2527; V. Sanz, R. Alcalde, M. Atilhan, S. Aparicio, *J. Mol. Mod.,* 2014, **20**, 1-14; S. Aparicio, M. Atilhan, *Energy Fuels,* 2010, **24**, 4989-5001.
48. S. Aparicio, M. Atilhan, *J. Chem. Phys. B* 2012, **116**, 9171-9185.
49. R. F. W Bader, *Atoms in Molecules: a Quantum Theory*. Oxford, **1990**.

50. E. R. Johnson, S. Keinan, P. Mori-Sánchez, J. Contreras-García, A. J. Cohen, W. Yang, *J. Am. Chem. Soc.,* 2010, **132**, 6498-6506.
51. T. Lu, F. Chen, *J. Comput. Chem.,* 2012, **33**, 580-592.
52. A. Postnikov. http://www.home.uni-osnabrueck.de/apostnik/download.html
53. Y. Zhao, D. G. Truhlar, *J. Chem. Theor. Comput.,* 2006, **3**, 289-300.
54. S. Cahangirov, S. Ciraci, *Phys. Rev. B.,* 2011, **83**, 165448 S. Cahangirov, M. Topsakal, E. Aktürk, H. Şahin, S. Ciraci, *Phys. Rev. Lett.,* 2009, **102**, 236804.

Table 1. Main molecular parameters for the most stables structures optimized at PBE/DZP and PBE-D2/DZP level for [CH][BE] ionic liquid. AIM parameters related with intermolecular interactions (electronic density, ρ, and its laplacian, $\nabla^2\rho$) as well as total charge over choline (q^+) and benzoate (q^-) ions computed according ChelpG / Hirshfeld schemes are also collected. See Figure 1 for labeling.

	PBE/DZP			PBE-D2/DZP		
	Length /Å	ρ / *a.u.*	$\nabla^2\rho$/ *a.u.*	Length/Å	ρ / *a.u.*	$\nabla^2\rho$/ *a.u.*
d_1	1.673	0.0668	0.1267	1.673	0.0668	0.1303
d_2	2.065	0.0221	0.0685	1.980	0.0265	0.0843
d_3	2.172	0.0193	0.0601	2.122	0.0213	0.0664
d_4	1.841	0.0356	0.1090	1.816	0.0382	0.1155
τ_1/º		0.0			0.0	
$q^+/e^{-\,a}$		0.69/0.50			0.68/0.48	

[a]For isolated [CH][BE] ionic liquid $q^+ = -q^-$.

Table 2. Main molecular parameters for the most stables structures optimized at PBE/DZP and PBE-D2/DZP levels. For [CH][BE]-Graphene system. AIM parameters related with intermolecular interactions (electronic density, ρ, and its laplacian, $\nabla^2\rho$) as well as total charge over choline (q^+), benzoate (q^-) ions and sheet (q^s) computed according to ChelpG / Hirshfeld schemes are also collected. See Figure 2 for labeling.

	PBE/DZP			PBE-D2/DZP		
	Length /Å	ρ / *a.u.*	$\nabla^2\rho$/ *a.u.*	Length/Å	ρ / *a.u.*	$\nabla^2\rho$/ *a.u.*
d_1	1.653	0.0702	0.1245	1.618	0.0772	0.1177
d_2	2.048	0.0230	0.0718	2.059	0.0222	0.0711
d_3	2.185	0.0188	0.0585	2.183	0.0191	0.0595
d_4	1.895	0.0314	0.0977	1.901	0.0309	0.0972
τ_1/º		0.0			0.0	
d_{eq}/Å		3.651			3.161	
d_5	3.601	0.0039	0.0119	3.126	0.0086	0.0275
d_6	3.507	0.0044	0.0135	3.198	0.0080	0.0271
d_7	3.768	0.0030	0.0092	3.240	0.0075	0.0256
d_8	3.749	0.0022	0.0071	3.305	0.0065	0.0239
d_9	3.154	0.0072	0.0251	2.930	0.0053	0.0194
d_{10}	2.762	0.0182	0.0354	2.485	0.0115	0.0446
$\sum$(BCP) [a]		0.0389	0.1022		0.0474	0.1861
$\sum$(RCP) [b]		0.0521	0.2316		0.0607	0.2142
CCP1		0.0037	0.0175		0.0603	0.2342
$\sum$(CCP) [c]		0.0032	0.0111		0.0040	0.0187
q^+/e^-		0.66/0.50			0.61/0.50	
q^-/e^-		-0.65/-0.48			-0.55/-0.47	
q^s/e^-		-0.01/-0.02			-0.06/-0.03	
$\Delta d_{C\text{-}C}$ [d]/Å		0.009			0.009	

[a/b/c] $\sum$(BCP) / $\sum$(RCP) / $\sum$(CCP) represents the sum of ρ or $\nabla^2\rho$ for those BCP /RCP /CCP related with intermolecular interactions between the IL and the sheet. [d]Difference value of C-C bonds corresponding to nanosheets after and before of the adsorption process.

Table 3. Main molecular parameters for the most stables structures optimized at PBE/DZP and PBE-D2/DZP levels. For [CH][BE]-Silicene system. AIM parameters related with intermolecular interactions (electronic density, ρ, and its laplacian, $\nabla^2\rho$) as well as total charge over choline (q^+), benzoate (q^-) ions and sheet (q^s) computed according to ChelpG / Hirshfeld schemes are also collected. See Figure 3 for labeling.

	PBE/DZP			PBE-D2/DZP		
	Length /Å	ρ / *a.u.*	$\nabla^2\rho$/ *a.u.*	Length/Å	ρ / *a.u.*	$\nabla^2\rho$/ *a.u.*
d_0	1.611	0.0605	0.1300	1.377	0.1103	0.0017
d_1	1.026	0.2835	-0.7304	1.086	0.2377	-0.7958
d_2	2.289	0.0133	0.0493	2.012	0.0229	0.0817
d_3	2.264	0.0154	0.0530	2.331	0.0139	0.0461
d_4	2.099	0.0192	0.0635	2.606	0.0071	0.0252
τ_1/º		15.3			-14.9	
d_{eq}/Å		3.649			3.178	
d_5	3.625	0.0059	0.0133	3.628	0.0061	0.0137
d_6	3.870	0.0043	0.0094	3.329	0.0118	0.0255
d_7	3.807	0.0045	0.0106	3.685	0.0058	0.0142
d_8	3.381	0.0076	0.0187	3.605	0.0065	0.0172
d_9	4.185	0.0022	0.0052	1.982	0.0071	0.0252
d_{10}	1.841	0.0835	0.3929	2.125	0.0528	0.0688
d_{11}	2.867	0.0117	0.0290	2.629	0.0170	0.0308
$\sum$(BCP) [a]		0.1196	0.4791		0.1072	0.1955
$\sum$(RCP) [b]		0.0666	0.2496		0.0967	0.3715
CCP1		0.0032	0.0144		0.0043	0.0205
$\sum$(CCP) [c]					0.0062	0.0176
q^+/e^-		0.63/0.72			0.71/0.80	
q^-/e^-		-0.57/-0.18			-0.65/-0.15	
q^s/e^-		-0.06/-0.54			-0.06/-0.65	
$\Delta d_{Si\text{-}Si}$ [d]/Å		0.002			0.007	

[a/b/c] $\sum$(BCP) / $\sum$(RCP) / $\sum$(CCP) represents the sum of ρ or $\nabla^2\rho$ for those BCP /RCP /CCP related with intermolecular interactions between the IL and the sheet. [d] Difference value of Si-Si bonds corresponding to nanosheets after and before of the adsorption process.

Table 4. Main molecular parameters for the most stables structures optimized at PBE/DZP and PBE-D2/DZP levels. For [CH][BE]-Germanene system. AIM parameters related with intermolecular interactions (electronic density, ρ, and its laplacian, $\nabla^2\rho$) as well as total charge over choline (q^+), benzoate (q^-) ions and sheet (q^s) computed according to Hirshfeld schemes are also collected. See Figure 4 for labeling.

	PBE/DZP			PBE-D2/DZP		
	Length /Å	ρ / *a.u.*	$\nabla^2\rho$/ *a.u.*	Length/Å	ρ / *a.u.*	$\nabla^2\rho$/ *a.u.*
d_0	1.079	0.2424	-0.8545	1.404	0.1023	0.0424
d_1	1.412	0.1015	0.0335	1.077	0.2433	-0.8680
d_2	2.070	0.0106	0.0346	2.309	0.0126	0.0479
d_3	2.469	0.0065	0.0151	2.287	0.0151	0.0523
d_4	3.071			2.064	0.0212	0.0683
τ_1/º		-16.7			5.9	
d_{eq}/Å		3.755			3.179	
d_5	3.617	0.0023	0.0061	3.310	0.0102	0.0240
d_6	3.747			3.039	0.0076	0.0228
d_7	2.318	0.0428	0.1160	3.218	0.0100	0.0257
d_8	2.409	0.0385	0.0992	2.045	0.0789	0.1860
d_9	3.032	0.0078	0.0181	2.740	0.0127	0.0273
d_{10}	3.356	0.0046	0.0113	2.935	0.0094	0.0211
$\sum$(BCP) [a]		0.0959	0.2507		0.1288	0.3070
$\sum$(RCP) [b]		0.1177	0.2249		0.1024	0.3646
CCP1		0.0038	0.0188		0.0647	0.0156
$\sum$(CCP) [c]		0.0056	0.0150		0.0087	0.0259
$q^{+\,d}/e^-$		0.81			0.75	
$q^{-\,d}/e^-$		-0.13			-0.01	
$q^{s\,d}\,e^-$		-0.68			-0.75	
$\Delta d_{Ge\text{-}Ge}$ [e]/Å		0.001			-0.009	

[a/b/c] $\sum$(BCP) / $\sum$(RCP) / $\sum$(CCP) represents the sum of ρ or $\nabla^2\rho$ for those BCP /RCP /CCP related with intermolecular interactions between the IL and the sheet. [d] ChelpG atomic charges were not computed since Breneman radii (which is needed to compute ChelpG charges) for Ge atom is not available in literature. [e]Difference value of Ge-Ge bonds corresponding to nanosheets after and before of the adsorption process.

Table 5. Main molecular parameters for the most stables structures optimized at PBE/DZP and PBE-D2/DZP levels. For [CH][BE]-Boron-Nitride system. AIM parameters related with intermolecular interactions (electronic density, ρ, and its laplacian, $\nabla^2\rho$) as well as total charge over choline (q^+), benzoate (q^-) ions and sheet (q^s) computed according to ChelpG / Hirshfeld schemes are also collected. See Figure 5 for labeling.

	PBE/DZP			PBE-D2/DZP		
	Length /Å	ρ / *a.u.*	$\nabla^2\rho$/ *a.u.*	Length/Å	ρ / *a.u.*	$\nabla^2\rho$/ *a.u.*
d_1	1.631	0.0743	0.1214	1.605	0.0803	0.1103
d_2	2.041	0.0233	0.0727	2.023	0.0240	0.0771
d_3	2.245	0.0167	0.0518	2.190	0.0189	0.0594
d_4	1.897	0.0314	0.0972	1.934	0.0287	0.0903
τ_1/º		1.7			3.8	
d_{eq}/Å		3.728			3.210	
d_5	3.763	0.0030	0.0089	3.288	0.0079	0.0270
d_6	3.760	0.0031	0.0096	3.171	0.0075	0.0231
d_7	3.876	0.0023	0.0067	3.168	0.0076	0.0243
d_8	3.800	0.0025	0.0074	3.254	0.0077	0.0237
d_9	3.900	0.0017	0.0057	2.992	0.0084	0.0242
d_{10}	3.152	0.0068	0.0194	2.595	0.0183	0.0497
d_{11}	2.666	0.0082	0.0278	2.542	0.0112	0.0379
$\sum$(BCP) [a]		0.0276	0.0855		0.0686	0.2099
$\sum$(RCP) [b]		0.0411	0.1864		0.0999	0.4232
CCP1		0.0038	0.0179		0.0040	0.0189
$\sum$(CCP) [c]					0.0072	0.0289
q^+/e^-		0.69/0.54			0.64/0.59	
q^-/e^-		-0.66/-0.43			-0.57/-0.33	
q^s/e^-		-0.03/-0.11			-0.07/-0.26	
$\Delta d_{B\text{-}N}$ [d]/Å		0.000			0.000	

[a/b/C] $\sum$(BCP) / $\sum$(RCP) / $\sum$(CCP) represents the sum of ρ or $\nabla^2\rho$ for those BCP /RCP /CCP related with intermolecular interactions between the IL and the sheet. [d] Difference value of B-N bonds corresponding to nanosheets after and before of the adsorption process.

Figure Captions.

Figure 1. Optimized structure at PBE/DZP level for isolated Choline Benzonate ([CH][BE]) along the main structural parameters related with intermolecular interactions. Atom colour code: (green) carbon, (red) oxygen, (blue) nitrogen and (white) hydrogen.

Figure 2. Top (up) and side (bottom) view for optimized structure at PBE/DZP level corresponding to [CH][BE]-Graphene (II [CH][Be]-C) system along structural parameters related with intermolecular interactions (left) and RGD iso-surfaces (right), whose green colour indicates van der Waals interactions. Atom colour code: (green) carbon, (red) oxygen, (blue) nitrogen and (white) hydrogen. Red and purple points stand for RCP and CCP, respectively, related with intermolecular interactions. BCP were omitted for simplicity.

Figure 3. Top (up) and side (bottom) view for optimized structure at PBE/DZP level corresponding to [CH][BE]-Silicene (III [CH][Be]-Si) system along structural parameters related with intermolecular interactions (left) and RGD iso-surfaces (right), whose green colour indicates van der Waals interactions. Atom colour code: (green) carbon, (red) oxygen, (blue) nitrogen, (white) hydrogen and (yellow) silicon. Red and purple points stand for RCP and CCP, respectively, related with intermolecular interactions. BCP were omitted for simplicity.

Figure 4. Top (up) and side (bottom) view for optimized structure at PBE/DZP level corresponding to [CH][BE]-Germanene (IV [CH][Be]-Be) system along structural parameters related with intermolecular interactions (left) and RGD iso-surfaces (right), whose green colour indicates van der Waals interactions. Atom colour code: (green) carbon, (red) oxygen, (blue) nitrogen, (white) hydrogen and (yellow) germanium. Red and purple points stand for RCP and CCP, respectively, related with intermolecular interactions. BCP were omitted for simplicity.

Figure 5. Top (up) and side (bottom) view for optimized structure at PBE/DZP level corresponding to [CH][BE]-Boron-Nitride (V [CH][Be]-BN) system along structural parameters related with intermolecular interactions (left) and RGD iso-surfaces (right), whose green colour indicates van der Waals interactions. Atom colour code: (green) carbon, (red) oxygen, (blue) nitrogen, (white) hydrogen and (pink) boron. Red and purple points stand for RCP and CCP, respectively, related with intermolecular interactions. BCP were omitted for simplicity.

Figure 6. Binding energies for the interaction between the both ions (BE_{IL}) at PBE/DZP (black) and PBE-D2/DZP level (red + blue) theoretical levels, wherein blue contributions stands for BE_{dis}.

Figure 7. Binding energies for the interaction between the IL and nanosheets ($BE_{IL\text{-}S}$) at PBE/DZP (black) and PBE-D2/DZP level (red + blue) theoretical levels, wherein blue bar stands for BE_{dis} contributions.

Figure 8. Density of States calculated at PBE/DZP theoretical level for pristine nanosheets (dotted line), [CH][BE] and [CH][BE]-nanosheets systems calculated at PBE/DZP levels (grey). Partial density of States (PDOS) for the ionic pair (green) as well as benzoate (red) and choline (blue) ions are also shown. Similar contours are obtained for PBE-D2 functional.

Figure 9. Molecular Orbital contours corresponding for the highest/lowest occupied/unoccupied molecular orbitals (HOMO/LUMO) located over the [CH][BE] ionic liquid calculated at PBE/DZP levels. Similar contours are obtained for PBE-D2 functional. HOMO and LUMO energies, along HOMO-LUMO energy differences are also indicated.

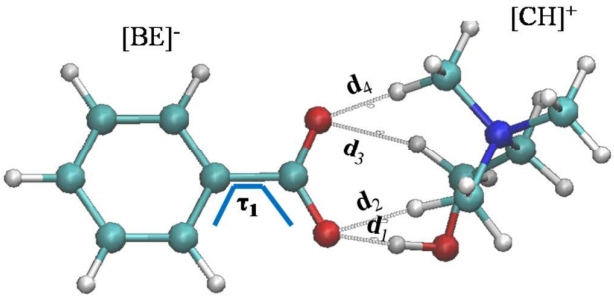

Figure 1.

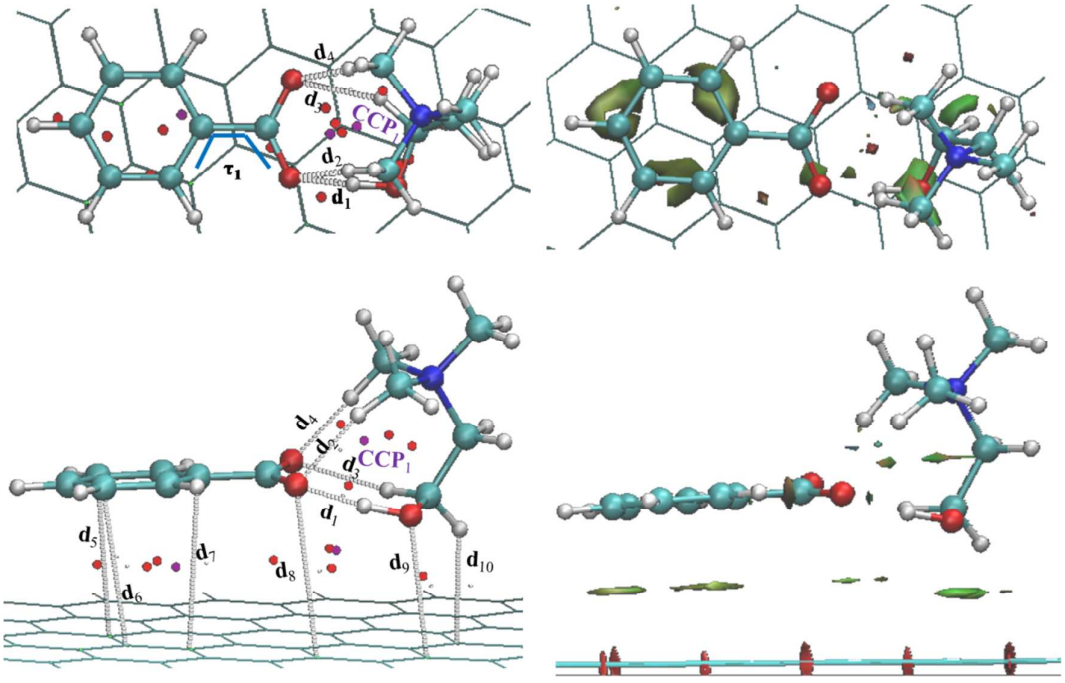

Figure 2.

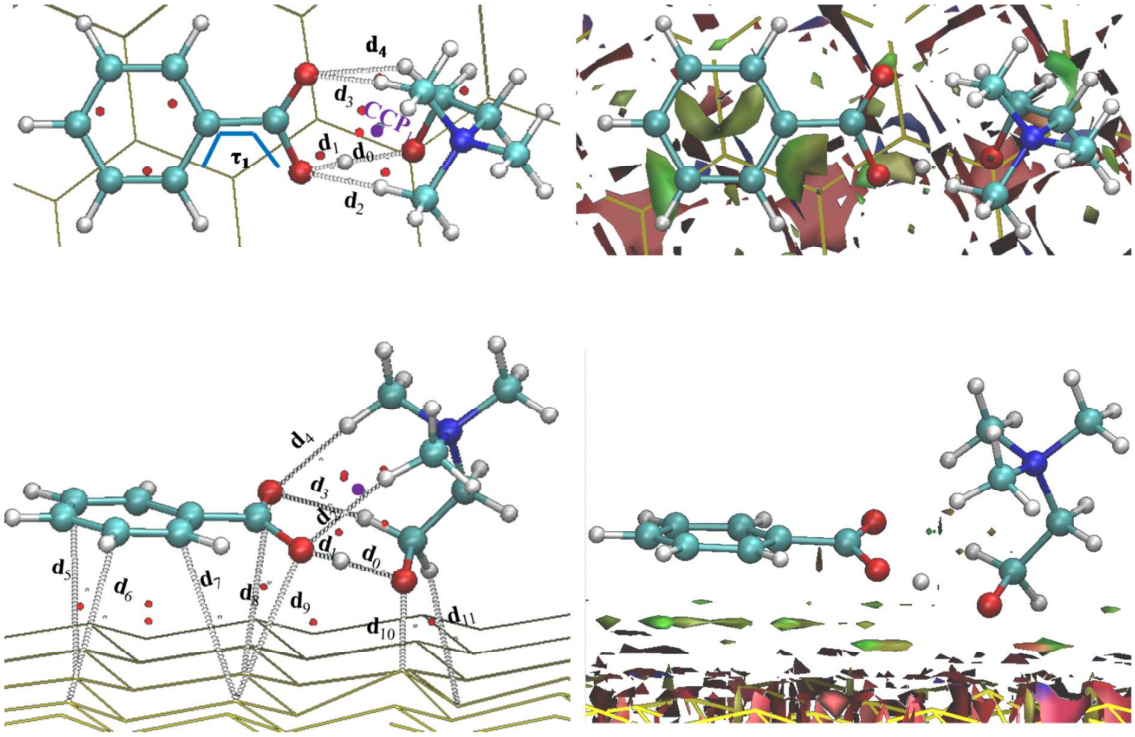

Figure 3.

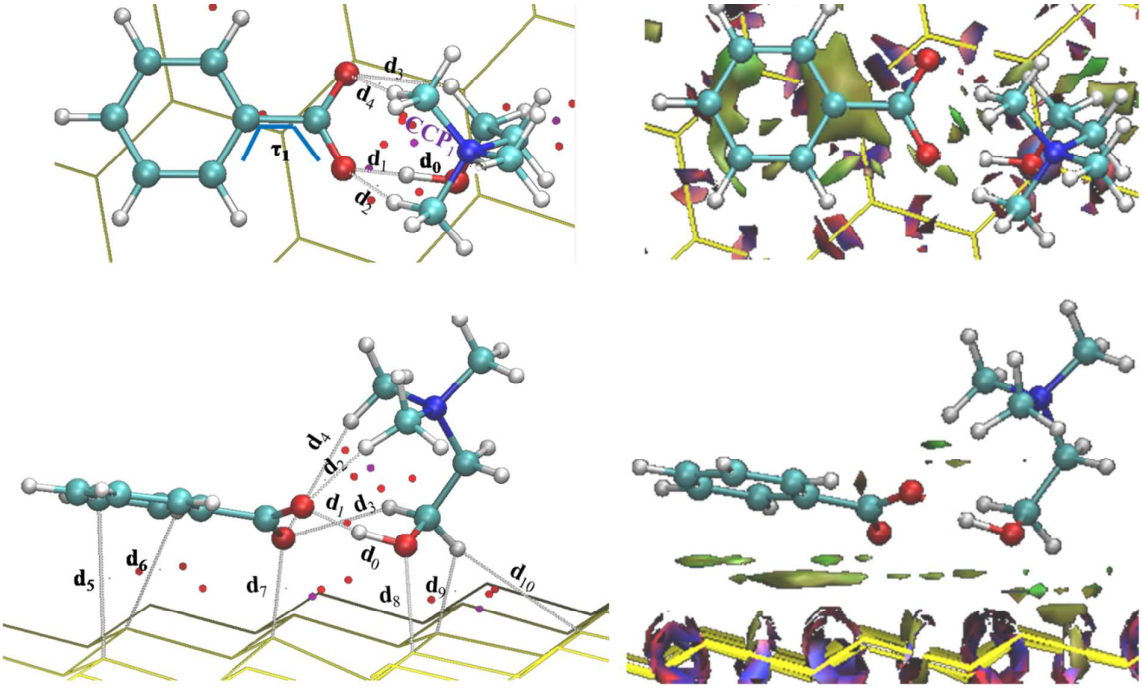

Figure 4.

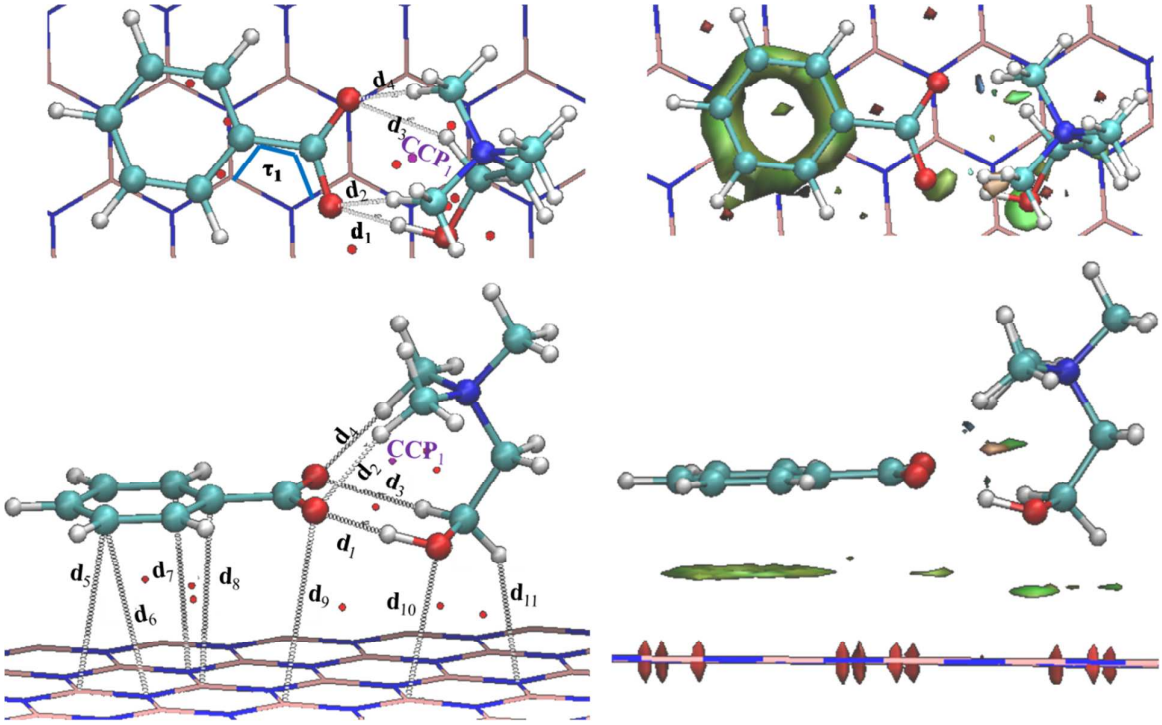

Figure 5.

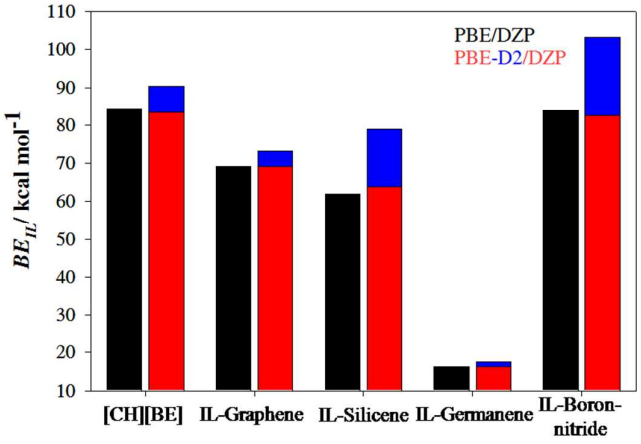

Figure 6.

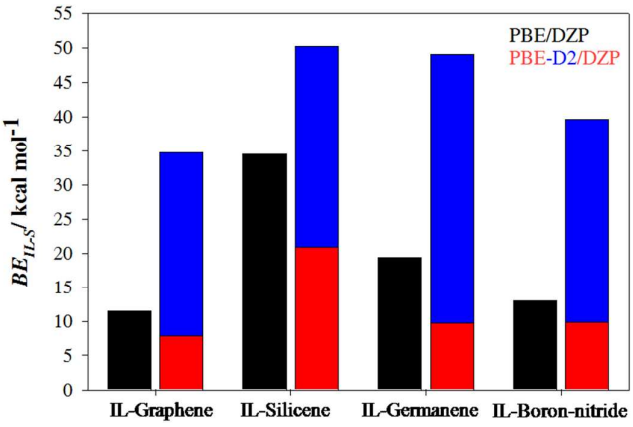

Figure 7.

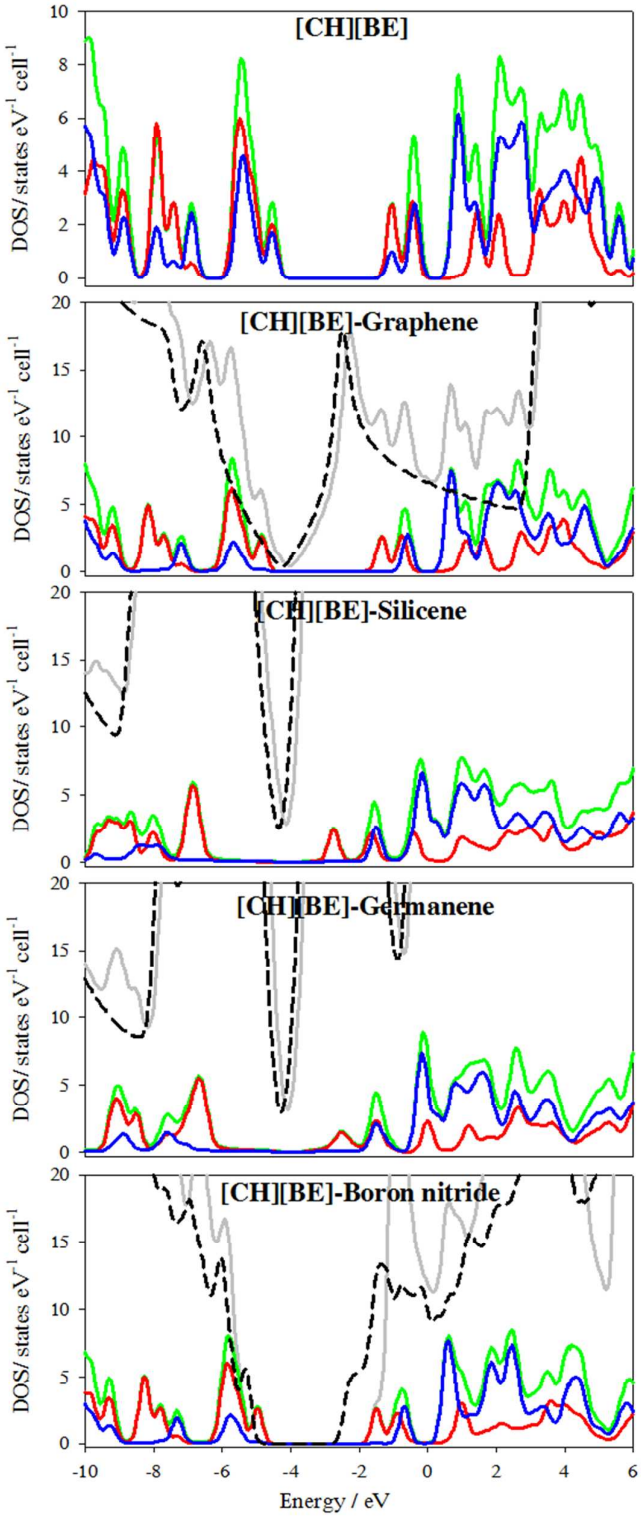

Figure 8.

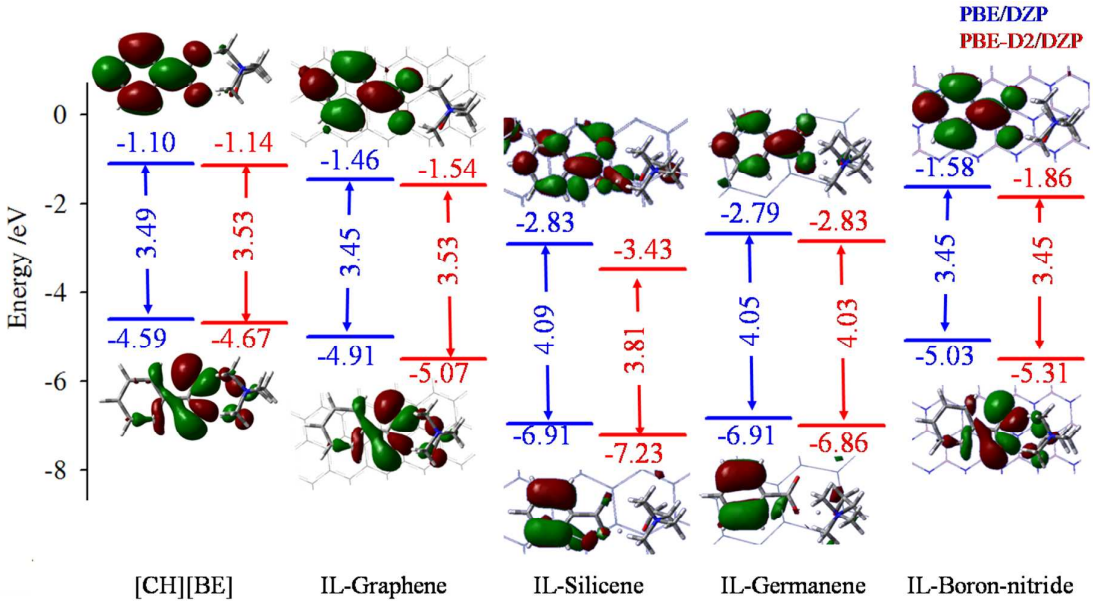

Figure 9.

Table of Contents Entry

This work assesses the adsorption of choline benzoate ionic liquid onto the surface of different nanosheets through DFT simulations.